Journal of Power Sources 196 (2011) 9391–9397

Contents lists available at ScienceDirect

Journal of Power Sources

journal homepage: www.elsevier.com/locate/jpowsour

Chaotic flow-based fuel cell built on counter-flow microfluidic network: Predicting the over-limiting current behavior

Jin Xuan[a], Dennis Y.C. Leung[a,*], Michael K.H. Leung[b], Huizhi Wang[a], Meng Ni[c]

[a] Department of Mechanical Engineering, The University of Hong Kong, Pokfulam Road, Hong Kong, China
[b] School of Energy and Environment, City University of Hong Kong, Hong Kong, China
[c] Department of Building and Real Estate, Hong Kong Polytechnic University, Hung Hom, Kowloon, Hong Kong, China

ARTICLE INFO

Article history:
Received 23 April 2011
Received in revised form 18 June 2011
Accepted 20 June 2011
Available online 25 June 2011

Keywords:
Lagrangian chaos
Microfluidics
Formic acid
Mass transport

ABSTRACT

The membraneless microfluidic fuel cell (MFC) is a promising micro-scale power source with potentially wide applications. MFC commonly relies on the co-laminar microfluidic platform in which redox streams flow in parallel in a microchannel. The nature of this cell architecture limits the mass transport inside the cell, often resulting in low power density. To overcome the issues, we propose an innovative concept of chaotic flow-based fuel cell (CFFC), which is built on a counter-flow microfluidic platform with the flow channel patterned with micro-ridges. A CFD/electrochemical model is used to predict the performance and investigate the underlay mechanism of the CFFC. Two theoretical upper bounds, i.e., the limiting current and limiting fuel conversion for conventional MFC, are derived. Through the results, it is found that the generation of chaotic flow inside the patterned activation zone enables the CFFC to exceed the theoretical limitations and work with over-limiting current for high-power output. Meanwhile, the interfacial mixing and crossover is minimized by the counter-flow microfluidics, allowing for over-limiting fuel conversion to useful electricity output. The achievement of unprecedented operating regime demonstrated in this study open up a new direction towards optimization, operating and design of the MFC.

1. Introduction

The membraneless microfluidic fuel cell (MFC) has recently drawn much research interest as a promising micro-scale power source for on-chip devices and microelectronics. The simple structure and working principle make MFC competitive among other types of micro-fuel cells, e.g., micro PEMFC and DMFC [1,2]. The original design of MFC, which is still widely adopted in recent published works [2–6], relies on the co-laminar microfluidic platform in which redox streams flow in parallel in a microchannel (typically in a Y-shape) with anode and cathode on the opposite channel walls. In the laminar regime, mass transport and fuel-oxidant mixing is limited to diffusive effects; thus restricted to the interfacial width. Since the two redox streams are naturally separated, the need for a membrane is eliminated. Meanwhile, protons can still efficiently transport between the two electrodes through electrolyte (Fig. 1a). Such kind of MFC is commonly specified as laminar flow-based fuel cell (LFFC) [5,6]. Reviews on the working principles, designs and recent development of LFFC can be found elsewhere [2,4].

To optimize the cell performance, one must minimize the mass transfer at the liquid–liquid interface to prevent the fuel crossover, while at the same time, mass transfer through the electrode concentration boundary layer should be enhanced for higher current density and fuel utilization. These two conflicting requirements pose enormous challenges to the manipulation of the transport patterns at such a small scale. For example, simply increase in the inlet flow rate may improve the cell current density and eliminate the fuel crossover. However, the fuel utilization will decline due to insufficient residence time for surface reactions. To date, seeking for an effective solution to control and optimize the transport behaviors in MFC is still an outstanding task.

Shear-driven chaotic flows have been noticed for their effects on the improvement of mass transport in microchannels [7–9]. Application to the MFCs can be found in Yoon et al. [10], reporting an increase in the fuel conversion rate up to 40% by patterning micro-ridges at the bottom of LFFC channel. However, the transverse secondary flows generated by the ridges may, at the same time, intensively mix the two streams within a short residence time [7,8]. Consequently, fatal LFFC operation will easily occur due to the sharp increase in parasitic current. However, in the experiment by Yoon et al. [10], the fuel crossover and parasitic effects were ignored by using a model redox of ferricyanide/ferrocyanide instead of a real fuel/oxidant couple. Therefore, their results may not be fully

* Corresponding author. Tel.: +852 2859 7911; fax: +852 2858 5415.
E-mail address: ycleung@hku.hk (D.Y.C. Leung).

0378-7753/$ – see front matter © 2011 Elsevier B.V. All rights reserved.
doi:10.1016/j.jpowsour.2011.06.065

Nomenclature

A_{cell}	interfacial area of the computational cell (m^2)
c	concentration (M)
C	fuel conversion rate
Da	Damköhler number
D_i	diffusivity of species i ($m^2\ s^{-1}$)
F	Faraday constant, 96,487 ($C\ mol^{-1}$)
h	channel height (m)
I	current (A)
j, j_0	current density, exchange current density ($A\ m^{-2}$)
L	length of the electrode (m)
M_i	molar mass of species i ($kg\ mol^{-1}$)
n	number of electrons exchanged at the rate-limiting step
n_t	number of total electrons exchanged
p	pressure (Pa)
R	universal gas constant ($8.314\ J\ mol^{-1}\ K^{-1}$)
S_i	source term of specie i ($kg\ s^{-1}\ m^{-3}$)
S_ϕ	source term in charge conservation ($V\ s^{-1}\ m^{-3}$)
T	temperature (K)
U, U_{trans}	velocity, transverse slip velocity ($m\ s^{-1}$)
V_{cell}	volume of the computational cell (m^3)
V_{op}	operating voltage (V)
w	channel width (m)
Y_i	mass fraction of species i

Greek letters

α	charge-transfer coefficient
η	overpotential (V)
ρ	density of the reactant streams ($kg\ m^{-3}$)
ϕ	potential (V)
σ	conductivity ($S\ m^{-1}$)
τ	stress tensor (Pa)
χ	reaction order
Θ_b	normalized bulk concentration

Subscripts

a	anode reaction
c	cathode reaction
f	formic acid
o	oxygen
lim	limiting
0	standard or reference

applicable to a practical LFFC. To overcome the interfacial mixing problem while maintaining enhanced mass transport to the electrode, we propose a novel concept of chaotic-flow based fuel cell (CFFC) that is built on a counter-flow microfluidic platform. In the counter-flow network, the activation zone (vicinity of electrode and micro-ridges) and mixing zone are spatio-temporally separated to facilitate control of the transport behaviors in microfluidics in order to fulfill different requirements on each functional region.

The CFFC is a brand new research area that is distinct from LFFC and any other types of fuel cells, and thus, need to be further investigated from device-level performance characteristics to microscopic level governing mechanisms. Further development for optimization of the cell design and operation is also urgent. Mathematical models have proven important in understanding and optimizing a new microfluidic device, such as CFFC. We have successfully developed a CFD/electrochemical model and used the model to investigate the micro-scale physico-electrochemical interactions in MFCs [11–13]. In this study, we extend and improve the model to be capable of modeling CFFC of air-breathing cathode design. The LFFC built on counter-flow microfluidic network, as reported in a recent communication [14], is also included in this study as a contrast for comparison. Through the modeling results, we predict that the CFFC can be operated at an over-limiting current condition, which is not possible for LFFC. Unprecedented current density and fuel conversion rate are predicted to exceed the theoretical upper bounds for conventional MFC. The results suggest that CFFC is a promising innovation which can contribute to the future development of MFC.

2. Methodology

2.1. Numerical model

2.1.1. Physical problem and computational domain

An illustration of the CFFC considered in this study is shown in Fig. 1b. The CFFC consists of an anodic activation region, a cathodic activation region and a mixing region. The fuel and cathodic supporting electrolyte are fed through opposite inlets of the anode and cathode, respectively. The two streams meet at the mixing region and the ionic charge transport takes place at the interface. Planar electrodes are assembled as the top boundaries of the cell. The cathode is a gas diffusion electrode that acquires oxygen from outside the cell. As shown in Fig. 1a, the charge transport pattern in CFFC is different from that in LLFC, but similar to that in a MFC using graphite rods as the electrodes [15]. To generate the chaotic flow, micro-ridges are patterned at the bottom of the cell to produce rotating eddies and vortices in the flow. The ridges are designed to repeating asymmetric patterns. As such, Lagrangian chaos will be generated [16,17]. Therefore, such microfluidic fuel cell is named as chaotic flow-based fuel cell.

The computational domain is built accordingly. As suggested by previous studies [8,16], the chaotic effect of the micro-ridges on the flow can be mimicked by replacing the detailed geometry of the ridges with a flat boundary with transverse slip velocity, as shown in Fig. 1c. The relationship between the slip velocity magnitude and the geometric parameters of the ridges is well stated elsewhere [8,18]. This simplification on the computational domain will not sacrifice the accuracy of the transport and chemical behaviors in the bulk flow and to the electrodes, which is the main focus in the study, although it may simplify the details on the patterned surface [16]. The treatment of slip boundaries has been justified elsewhere [8,16,18].

2.1.2. Electrochemical model

Considering an air-breathing CFFC running on formic acid, the electrochemical system becomes

$$\text{Anodereaction}: 2HCOOH \rightarrow 2CO_2 + 4H^+ + 4e^-; \quad (1)$$

$$\text{Cathodereaction}: O_2 + 4H^+ + 4e^- \rightarrow 2H_2O. \quad (2)$$

For both electrodes, their reverse reactions are negligible during MFC operation [19]. Therefore, their reaction rates can be expressed by Tafel law.

$$j_a = j_{a,0}\left(\frac{c_f}{c_{f,0}}\right)^{\chi_a} \exp\left(\frac{\alpha_a n_a F \eta_a}{RT}\right) \quad (3)$$

$$j_c = -j_{c,0}\left(\frac{c_o}{c_{o,0}}\right)^{\chi_c} \exp\left(-\frac{\alpha_c n_c F \eta_c}{RT}\right) \quad (4)$$

In the above equations, there are several unknown variables, i.e., fuel and oxidant concentration at the electrode surface and electrode overpotential, which can be derived from subsequent CFD model. Particularly, the oxygen concentration at the electrode surface is given as a constant equivalent to its fraction in the air. It is because a recent study [20] revealed that the oxygen concentra-

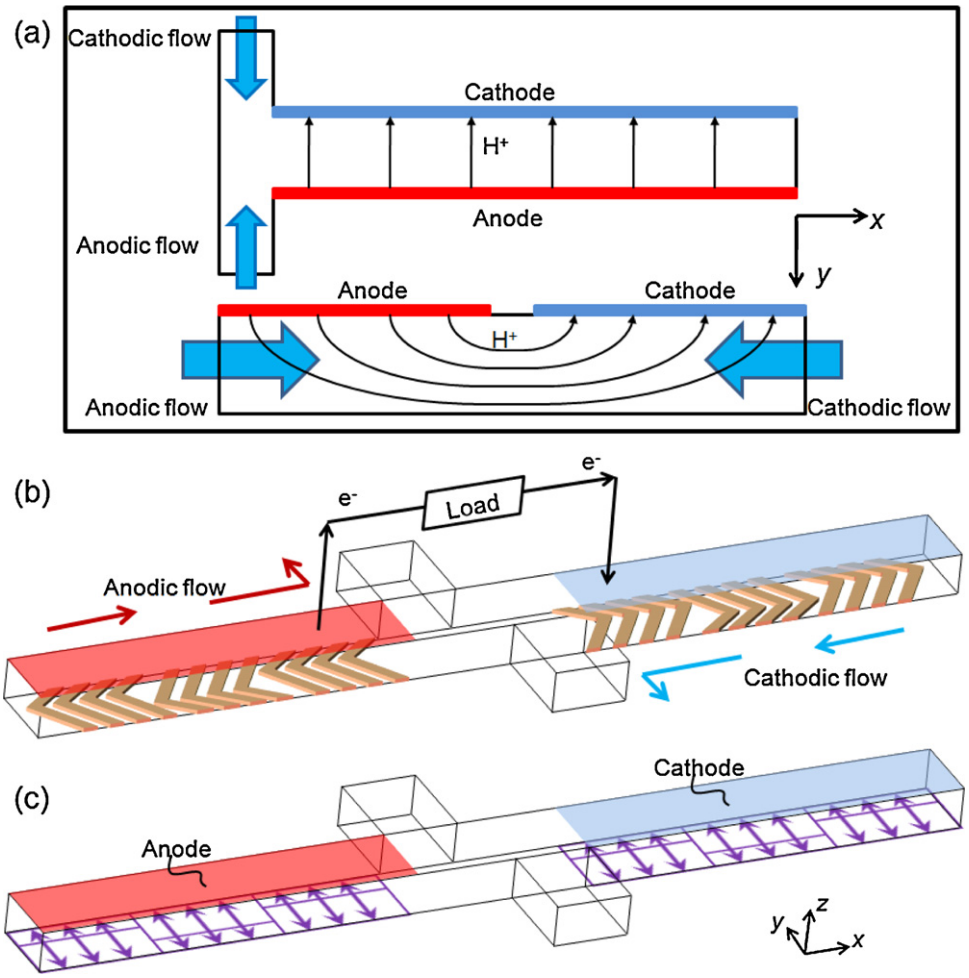

Fig. 1. Illustration of CFFC: (a) working principles and charge transport in co-laminar and counter-flow MFCs, (b) detailed geometry, and (c) approximation adopting flat boundary with transverse slip velocities.

tion polarization at the cathode of MFC is negligible, providing the external oxygen supply to the cathode is sufficient.

2.1.3. CFD model

In the CFD model, the coupled continuity equation, Navier–Stokes equations, species transport equation and electric potential equation are solved in the 3D domain.

$$\nabla \cdot (\rho U) = 0 \tag{5}$$

$$\nabla \cdot (\rho UU) = -\nabla p + \nabla \cdot \tau \tag{6}$$

$$\nabla \cdot (\rho UY_i) - \nabla \cdot (\rho D_i \nabla Y_i) = S_i \tag{7}$$

$$\sigma \nabla^2 \phi = S_\phi \tag{8}$$

The species transport equation is solved for formic acid. The mass balance is ensured by assuming another species of "bulk mixture", whose mass fraction is set to be unity minus the mass fractions of formic acid. The source/sink terms, S_i and S_ϕ, correspond to the volumetric-basis species depletion and current production due to the electrochemical reactions, respectively. They are confined in a layer of control volumes neighboring the electrode/electrolyte interface and zero in other computational zones.

$$S_i = -\frac{M_i A_{\text{cell}}}{n_{t,i} F V_{\text{cell}}} j_i \tag{9}$$

$$S_\phi = \frac{A_{\text{cell}}}{V_{\text{cell}}} j_i \tag{10}$$

2.1.4. Boundary conditions

The boundary conditions of the above equations include non-slip, non-permeable conditions at channel walls and electrodes, designated slip velocity for mimic ridged boundaries, designated velocities and concentrations at inlets, and the pressure outlet, etc. Note that zero-flux boundaries are specified to the electrodes here for the species because any production or consumption has been included as a source term appearing in the governing equations.

2.1.5. Numerical procedures

Input parameters of the model are summarized in Table 1, which have been adopted in our previous studies [13]. Finite Volume Method code FLUENT 6.3 [21] is used to solve the equations numerically. To minimize the numerical diffusion, structural meshes under strict grid independence control, and higher order discretization schemes are used, i.e., the semi-implicit method for pressure linked equations (SIMPLE) algorithm with the quadratic upwind interpolation of convective kinematics (QUICK) scheme, adopted for the pressure–velocity coupling and discretization schemes.

2.2. Limiting current and fuel conversion

In the analysis, dimensionless velocity and current are introduced, enabling the comparison of microfluidic fuel cells with

Table 1
Key input parameters [13].

Parameter	Value
Electrode kinetics	
α_a	0.5
α_c	0.497
$j_{a,0}$ (A m^{-2})	0.1194
$j_{c,0}$ (A m^{-2})	3.1×10^{-7}
n_a	1
n_c	1
χ_a	1
χ_c	1
Fluidic properties	
ρ (kg m^{-3})	1008.6
μ (kg m^{-1} s^{-1})	0.001 (water)
σ (S m^{-1})	0.4
D_f (m^2 s^{-1})	5×10^{-10}
Inlet conditions	
c_f (M)	1.05
T (K)	297

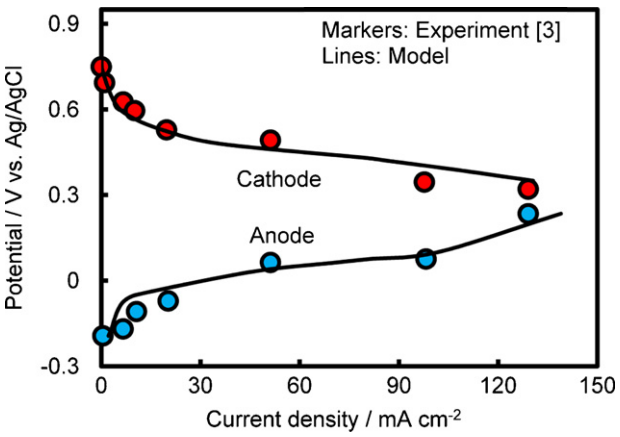

Fig. 2. Comparison between experimental data [3] and model results on the cell performance.

different operating conditions and geometries. They are defined as:

$$I^* = I\frac{2w}{n_t F h L c_{in} D_i} \tag{11}$$

and

$$U^* = U\frac{4w^2}{LD} \tag{12}$$

The limiting current of a fuel cell is usually defined as the point in the polarization curve where its shape becomes vertical, and no further increase in current can be obtained regardless of the applied overpotential, due to insufficient mass transport rate compared to the electrode reaction rate. In LFFC, the limiting current correlates with inlet velocity [15,22],

$$I^*_{\text{lim}} = \begin{cases} \frac{1}{2}U^* & (U^* < 6.859) \\ 1.849U^{*1/3} & (U^* \geq 6.859) \end{cases} \tag{13}$$

We further discuss the fuel conversion rate as a function of U^* in a LFFC. The hydrodynamics in the cell is pressure-driven flow. Therefore, the bulk concentration of the fuel when the flow leaves the activation region, Θ_b, can be analytically solved [23].

$$\Theta_b = \exp\left(-\frac{4\lambda_1^2}{6U^*}\right) \tag{14}$$

where the first eigenvalue, λ_1, is determined numerically and fitted approximately in the form of [23]

$$\frac{\lambda_1^2}{6} = 1.4304(1 - \exp(-0.68Da)) + \exp\left(\frac{-5.77}{Da}\right) \tag{15}$$

At the critical condition when $I = I_{\text{lim}}$, the Damköhler number (Da) for anode becomes infinity. At that condition, Θ_b reaches its

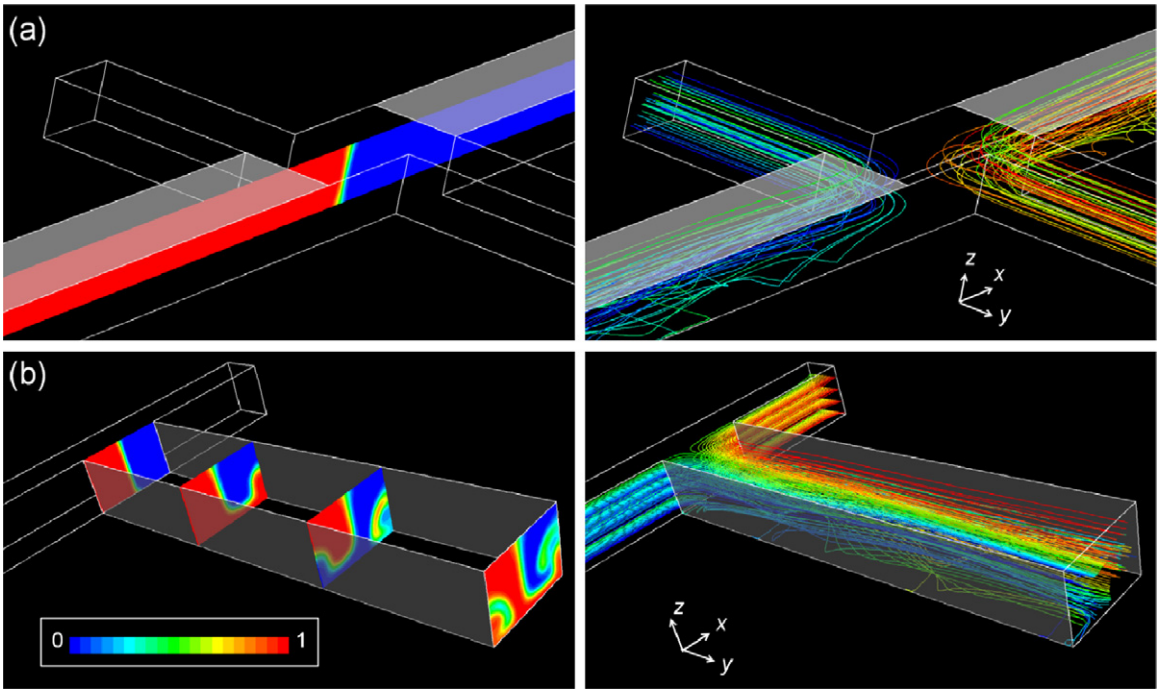

Fig. 3. Comparison of fuel distribution (left, unit: M) and flow patterns (right, colored by the coordinates of the origins of the patterns) for CFFCs based on (a) counter-flow platform and (b) co-laminar flow platform.

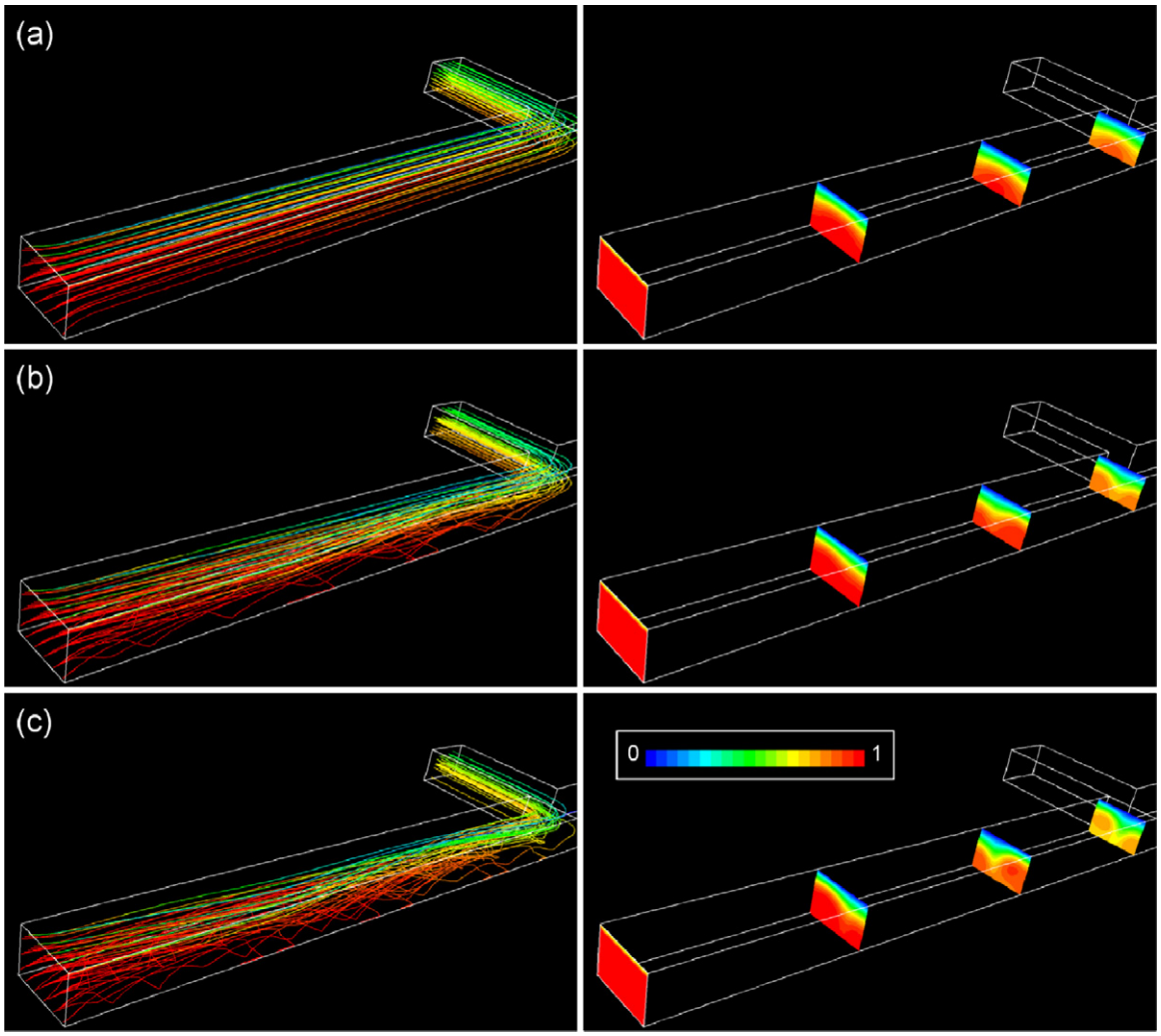

Fig. 4. Comparison of flow patterns (left, colored by fuel concentration at local position) and fuel distribution (right, unit: M) for CFFC with U_{trans}/U equal to (a) 0, (b) 0.5, and (c) 1.

minimum value and the corresponding limiting fuel conversion rate, C_{lim}, can be expressed in the way of

$$C_{lim} = 1 - \Theta_b = 1 - \exp\left(\frac{9.7216}{U^*}\right) \quad (16)$$

So far, we have reviewed and derived two theoretical upper bounds for the operation of LFFC, i.e., I_{lim} and C_{lim}. Based on that, two operating conditions of a microfluidic fuel cell can be defined, which are under-limiting current condition ($I < I_{lim}$ and $C < C_{lim}$) and over-limiting current condition ($I > I_{lim}$ and $C > C_{lim}$). Normally, for practical operation of LFFC, various losses lead to the cell performance deviating from the theoretical upper bounds to an under-limiting current condition. In the subsequent sections, we demonstrate that the operation of CFFC outperforms the theoretical upper bounds posed on LFFC and unprecedented high current density and fuel conversion are obtained.

3. Results and discussion

3.1. Model validation

Validation of the model is conducted by comparing the individual anode and cathode performances of an air-breathing LFFC obtained from the model and experimental results [3]. The geometric and operating input parameters of the simulation follow the experimental study by Jayashree et al. [3]. Fig. 2 shows the results of the comparison, from which, reasonable agreement can be found. Moreover, implementations of the validation of the present model have also been conducted several times in our previous works. We have shown that the model is able to accurately predict the convection–diffusion-reaction interactions [11,12] and electrochemical performance [12,13] of microfluidic fuel cells.

3.2. Interfacial transport

As mentioned earlier, the chaotic flows in the MFC may mix the anodic and cathodic streams and cause fuel crossover problem. Therefore, it is important to evaluate the interfacial mixing patterns of the CFFC to prove the feasibility of the concept. Fig. 3 compares the hydrodynamic conditions and interfacial transport patterns in CFFCs based on counter-flow and co-laminar flow platforms under a velocity $U_{trans}/U = 0.5$. For clear illustration and explanation, the electrode reactions are not included at the current stage (i.e., $I = 0$). It is found that for CFFC based on counter-flow network, the interfacial mixing is well-controlled. Within all cases studied in this paper, no crossover of the fuel is observed. It is because the transverse secondary flows generated by micro-ridges are parallel to the interface of the two streams, and, thus, will not contribute to

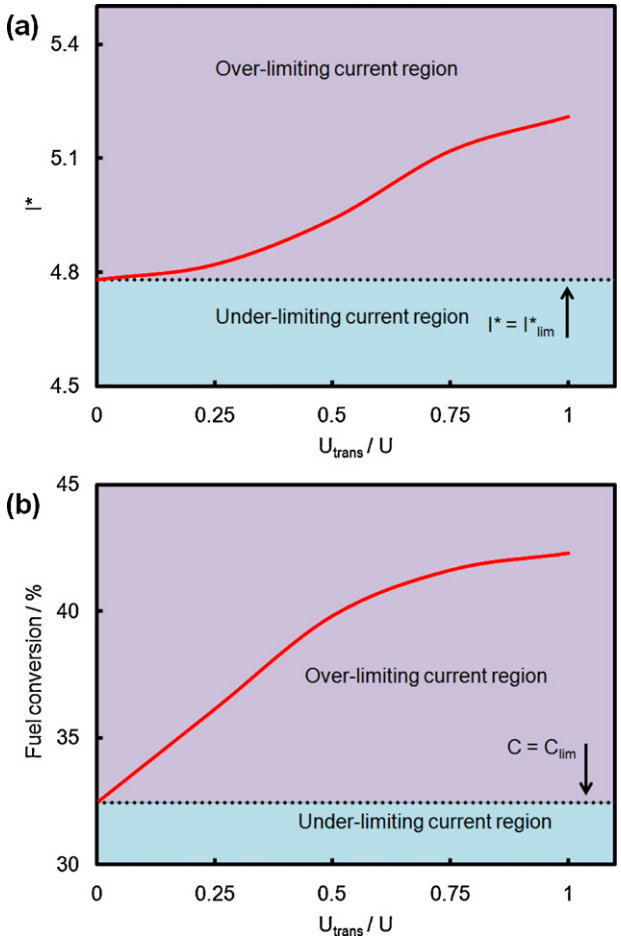

Fig. 5. (a) Dimensionless current and (b) fuel conversion versus U_{trans}/U.

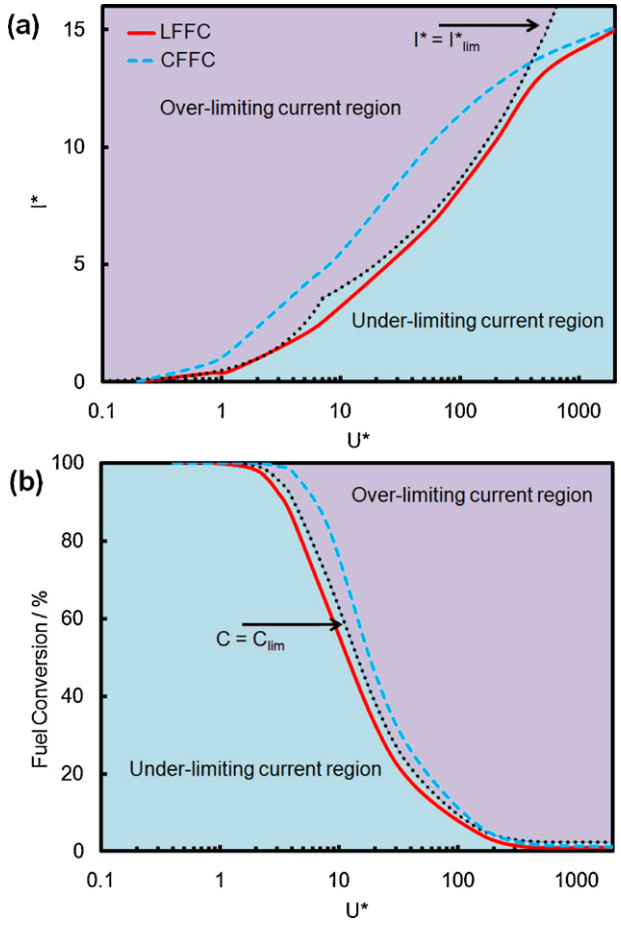

Fig. 6. (a) Dimensionless current and (b) fuel conversion versus U.

the interfacial mixing. Moreover, due to the dominating viscous effects, the chaotic flow will become a steady laminar flow at the mixing region, once it leaves the patterned activation region. This hydrodynamic behavior benefits the minimization of the interfacial mixing by eliminating the harmful convective flux at the stream interface. On the contrary, CFFC based on co-laminar flow network shows serious mixing and fuel crossover problems inside the channel, which is similar with a microfluidic mixer [16,17]. The results indicate that the counter-flow network is potentially a much more promising platform to realize the CFFC concept.

3.3. Over-limiting current behavior

We consider a CFFC with $L = 5$ mm, $w = 0.5$ mm, $U = 1$ mm s^{-1}, and $V_{op} = 0.1$ V. For air-breathing MFC, the cell current density and fuel conversion is primarily determined by the anode part [5,10,24]. Fig. 4 shows the flow patterns and fuel concentration field in the anode activation region of the CFFC at $U_{trans}/U = 0$, 0.5 and 1, referring to laminar, low chaotic and high chaotic flow regimes, respectively. It is found that at $U_{trans}/U = 0$ (i.e., equivalent to a LFFC), the flow in the channel is laminar and the cell is working at limiting current condition with a gradually developed concentration boundary layer adjunct to the electrode. With the increase in the U_{trans}/U, the secondary helical flow will be generated by the patterned ridges and the flow in the activation zone becomes more chaotic (Fig. 4 left column). At the same time, mass transfer to the electrode is enhanced in the channel, leading to steeper concentration variation in the boundary layer and low fraction of the fuel in the bulk (Fig. 4 right column). Therefore, as shown in Fig. 5, I^* and C are enhanced with the increase in the U_{trans}/U, resulting in an over-limiting current condition in which $I > I_{lim}$ and $C > C_{lim}$. Essentially, the performance exceeding theoretical upper bounds can be attributed to the benefit of the chaotic flow regime in the CFFC, since the two theoretical upper bounds are calculated based on pressure-driven laminar flow condition. Note that the current density and fuel conversion rate can be simultaneously enhanced by increasing U_{trans}/U by proper design of the micro-ridge patterning, which does not suffer from the common trade-off limitation in LFFC optimization [24].

We then examine the effect of operating flow rate on the performance of the CFFC. In the model, the design and operating parameters of the CFFC are set to be identical as the previous case, except that U_{trans}/U is fixed to 1 and U^* becomes a variable. A LFFC based on the counter-flow microfluidic platform with the same geometry and operation condition but without patterning is included for comparison. Fig. 6a and b shows the change of I^* and C against various U^*, respectively. The over-limiting current and under-limiting current regions are distinguished by identifying I^*_{lim} and C_{lim} according to Eqs. (13) and (16). It is observed that, generally, the current density increases while the fuel conversion decreases with increasing inlet velocity for both the CFFC and LFFC. However, the CFFC could exceed the critical values of I^*_{lim} and C_{lim} to work at over-limiting current region in a wide range of operating flow rate, while the LFFC can only be operated at under-limiting current region. The advantage of CFFC is clearly shown. At higher flow rate condition, both curves for CFFC and LFFC return to the under-limiting current region. It is because the transport limitation is not

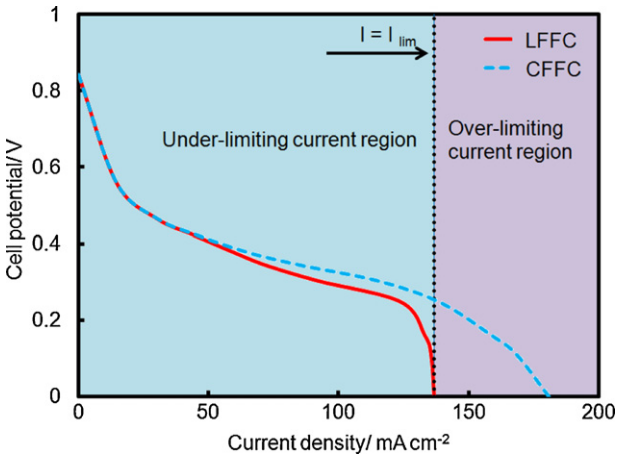

Fig. 7. Polarization curve for LFFC and CFFC based on counter-flow network.

reached with high inlet velocity: high flow rate leads to high mass transport to the electrode; when the mass transport rate becomes faster than the surface reaction rate, electrochemical and electrical aspects of the cell will play the primary role to determine the cell performance, i.e., non-ideal reaction kinetics and ohmic resistance becomes significant [15]. It indicates that using chaotic flow to enhance the performance of MFC will show distinct effect when the mass transport in the cell is critical, i.e., at high current condition and low flow rate. On the contrary, at activation and ohmic regime of cell operation, the strategy becomes less significant. It practice, to approach ultra high fuel utilization (i.e., near 100%), the cell must be operated at low flow rate and high current condition, under which condition the CFFC technique would be particularly useful.

Finally, the *J–V* characteristics of the CFFC and LFFC on counter-flow network are predicted and compared in Fig. 7. It is found that at high current operating condition, the performance of LFFC is limited by mass transport to the anode, resulting in limiting current behavior. It means that the cell current is restrained by the theoretical upper bound, I_{lim}, and becomes irrelevant to the operating potential. Similarly, the *J–V* curve for CFFC yields the same trend as the one for LFFC at low to medium current conditions. Yet, the improved performance of CFFC becomes obvious at high current condition when the concentration overpotential turns significant. Furthermore, the operating condition extends to the over-limiting current region without the restrain by the theoretical limitation, i.e., I_{lim}. From the results, it is calculated that the CFFC design enables increase of maximum current density from 137 mA cm^{-2} to 181 mA cm^{-2}, and maximum power density from 30 mW cm^{-2} to 35 mW cm^{-2}.

However, both cell potentials of LFFC and CFFC drop rapidly with the increase in the current density at low to medium current operating condition, which can be mainly attributed to the high ohmic overpotential involved. It is because the way of arrangement of two electrodes in counter-flow platform causes longer route for the charged ions to transfer between two electrodes compared with its co-laminar flow counterpart (Fig. 1a). To minimize the ohmic loss, the electrode length shall be reduced and cell scale shall be miniaturized accordingly. A decrease in the electrode length in the cell design can lead to an increase in the cell current density since most of the current are collected within the region near the inlet [24]. However, the fuel utilization will be lowered due to the reduction in the residence time of reaction. Since the fuel conversion rate can be compensated by adopting higher U_{trans}/U or lower U in CFFC operation, the issue of low fuel utilization would be partly overcome.

4. Conclusion

Manipulation of the transport patterns in membraneless microfluidic fuel cell is of great importance to obtain high performance. Yet, rare successful attempts have been reported. This study proposed a novel concept of chaotic flow-based fuel cell built on counter-flow microfluidic platform to fulfill the research gap. The design benefits from the separation of the activation zone and mixing zone, which facilitates to accurately manipulate the transport behaviors for each important physico-electrochemical process. For example, the mass transport at activation zone and mixing zone will not influence each other. A CFD/electrochemical model is developed to study the performance and underlay mechanism of the CFFC. Moreover, two theoretical upper bounds (i.e., the limiting current and limiting fuel conversion) for conventional MFC have been derived. We have predicted that the CFFC can be operated at the over-limiting current condition to exceed the theoretical upper bounds and achieve unprecedented performance of high current density and high fuel conversion rate. The unique operating regime enables simultaneous optimization of current density, fuel utilization and interfacial mixing by proper design of the micro-ridge patterning without the trade-off limitation. Similar achievement has never been reported in the literature. Therefore, the study opens up a new direction for MFC research.

Acknowledgement

The research work presented in this paper is supported by the CRCG of the University of Hong Kong.

References

[1] R. Ferrigno, A.D. Stroock, T.D. Clark, M. Mayer, G.M. Whitesides, J. Am. Chem. Soc. 124 (2002) 12930–12931.
[2] S.A.M. Shaegh, N.T. Nguyen, S.H. Chan, Int. J. Hydrogen Energy 36 (2011) 5675–5694.
[3] R.S. Jayashree, L. Gancs, E.R. Choban, A. Primak, D. Natarajan, L.J. Markoski, P.J.A. Kenis, J. Am. Chem. Soc. 127 (2005) 16758–16759.
[4] E. Kjeang, N. Djilali, D. Sinton, J. Power Sources 186 (2009) 353–369.
[5] J. Lee, K.G. Lim, G.T.R. Palmore, A. Triathi, Anal. Chem. 79 (2007) 7301–7307.
[6] E. Kjeang, B.T. Proctor, A.G. Brolo, D.A. Harrington, N. Djilali, D. Sinton, Electrochim. Acta 52 (2007) 4942–4946.
[7] A.D. Stroock, S.K.W. Dertinger, A. Ajdari, I. Mezic, H.A. Stone, G.M. Whitesides, Science 295 (2002) 647–651.
[8] A.D. Stroock, G.J. McGraw, Philos. Trans. R. Soc. Lond. Ser. A 362 (2004) 971–986.
[9] B.-U. Moon, S. Koster, K.J.C. Wientjes, R.M. Kwapiszewski, A.J.M. Schoonen, B.H.C. Westerink, E. Verpoorte, Anal. Chem. 82 (2010) 6756–6763.
[10] S.K. Yoon, G.W. Fichtl, P.J.A. Kenis, Lab. Chip 6 (2006) 1516–1524.
[11] J. Xuan, M.K.H. Leung, D.Y.C. Leung, M. Ni, Chem. Eng. J. 171 (2011) 216–223.
[12] J. Xuan, M.K.H. Leung, D.Y.C. Leung, H. Wang, Appl. Energy, in press.
[13] J. Xuan, M.K.H. Leung, D.Y.C. Leung, H. Wang, Appl. Energy; in press.
[14] K.S. Salloum, J.D. Posner, J. Power Sources 195 (2010) 6941–6944.
[15] E. Kjeang, J. McKechnie, D. Sinton, N. Djilali, J. Power Sources 168 (2007) 379–390.
[16] J.D. Kirtland, G.J. McGraw, A.D. Stroock, Phys. Fluids 18 (2006) 073602.
[17] A.D. Stroock, S.K. Dertinger, G.M. Whitesides, A. Ajdari, Anal. Chem. 74 (2002) 5306–5312.
[18] J.D. Kirtland, C.R. Siegel, A.D. Stroock, New J. Phys. 11 (2009) 075028.
[19] D.H. Ahmed, H.B. Park, H.J. Sung, J. Power Sources 185 (2008) 143–152.
[20] S.A.M. Shaegh, N.T. Nguyen, S.H. Chan, J. Micromech. Microeng. 20 (2010) 105008.
[21] Fluent Inc., Fluent User's Guide Version 6.3, Lebanon, 2003.
[22] E. Kjeang, B. Roesch, J. McKechnie, D.A. Harrington, N. Djilali, D. Sinton, Microfluid. Nanofluid. 3 (2007) 403–416.
[23] T. Gervais, K.F. Jensen, Chem. Eng. Sci. 61 (2006) 1102–1121.
[24] R.S. Jayashree, S.K. Yoon, F.R. Brushett, P.O. Lopez-Montesinos, D. Natarajan, L.J. Markoski, P.J.A. Kenis, J. Power Sources 195 (2010) 3569–3578.